

General Purpose Electrostatic Embedding Potential

Peter V. Sushko*,†,‡ and Igor V. Abarenkov§

*Department of Physics and Astronomy and London Centre for Nanotechnology,
University College London, Gower Street, London WC1E 6BT, United Kingdom, WPI
Advanced Institute for Materials Research, Tohoku University, Sendai 980-8577,
Japan, and Department of Physics, St. Petersburg State University,
St. Petersburg 198504, Russia*

Received September 10, 2009

Abstract: We present a method and a computer code for accurate calculation of electrostatic potential in an arbitrary crystalline lattice modeled using a finite system. The method is based on complementing a lattice unit cell with a set of point charges in order to annihilate simultaneously all components of *any number* of the lowest multipole moments. The positions and the values of the complementary charges are determined analytically. The electrostatic potential produced by each modified cell is short range, and the corresponding lattice series converges absolutely, which makes it convenient to use in embedded cluster calculations of solids, surfaces, and low-dimensional structures. The method is illustrated by application to the rutile TiO_2 and α -quartz SiO_2 lattices and to those of several complex minerals.

1. Introduction

In embedded cluster and quantum mechanics/molecular mechanics (QM/MM) methods, a QM description of a part of the system, called a “region of interest”, is combined with the empirical description of its surroundings. These methods are particularly advantageous to use in cases where electronic states, associated with the region of interest, and those, associated with its environment, are separated in space and in energy. Numerous implementations of these techniques (see, for example, refs 1–14) and their applications to studies of large organic molecules,¹⁵ solutions,^{13,16,17} nanoparticles,¹⁸ molecular crystals,^{19,20} excitons^{21,22} and reactions and properties of defects^{23–27} have been reported.

The QM/MM methods often use a finite system (which will be referred to as a *nanocluster* or NC) to model the bulk, the surfaces, and the complex interfaces in crystals. It is well-known that the electrostatic potential (EP) inside a finite system depends on the choice of the structural element used to construct it. We illustrate this idea on the example of a nanocluster constructed as a 5×5 extension of a crystal

unit cell, as shown schematically in Figure 1a. If the unit cell has zero dipole (D) and nonzero quadrupole (Q) moments, the electrostatic potential V in the inner region of the nanocluster, indicated with a circle, depends on the details of the nanocluster structure. As the size of the nanocluster increases, the potential converges to the Ewald potential shifted by a constant, which can adopt any value from $-\infty$ to $+\infty$, depending on the shape of the nanocluster.

This creates problems if *absolute* positions of energy levels need to be calculated. In particular, the values of the ionization energies and the electron affinities, calculated for surface defects, depend on the EP in a nanocluster modeling this surface and, therefore, on the particular way the nanocluster is constructed. Accurate prediction of these properties is important for understanding a wide range of processes. For example, theoretical prediction of the MgO (001) surface ionization potential^{5,28} has helped to map out the energy levels of surface oxygen vacancies, hydrogen defects, and nanoscale structural defects,^{5,29,30} with respect to both the top of the surface valence band and the vacuum level. These theoretical results have been used successfully to develop mechanisms of complex photoinduced processes including charge transfer,³¹ site-selective chemical reactions,³² and atom desorption.^{33,34} Recent similar results obtained for silica surfaces²⁵ may need to be reconsidered

* Corresponding author. E-mail: p.sushko@ucl.ac.uk.

† University College London.

‡ Tohoku University.

§ St. Petersburg State University.

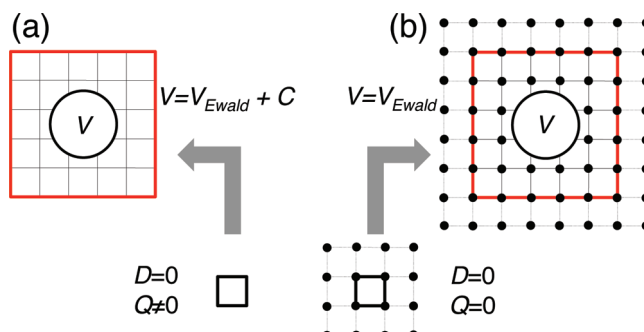


Figure 1. Electrostatic potential V in the inner region of a nanocluster (top panels) depends on the lattice unit cell (bottom panels) used to generate it. (a) If the unit cell has zero dipole (D) and nonzero quadrupole (Q) moments, then $V(r)$ converges to $V_{\text{Ewald}}(r) + C$ with increasing size of the nanocluster, where constant C can adopt any value depending on the shape of the nanocluster. (b) If the unit cell is complemented with point charges so as both $D = 0$ and $Q = 0$, $V(r)$ converges to $V_{\text{Ewald}}(r)$ absolutely. The complementary charges (bold dots) are situated at the points equivalent to the unit cell corners. The boundaries of the nanocluster are indicated with bold solid lines.

because, unlike the MgO case, structural elements used to generate silica nanoclusters possessed nonzero quadrupole moments. The ambiguity in the values of the EP makes it difficult to set up a common reference for the bulk and surface defects in the same system and to compare results obtained for defects in different materials.

In this work, we suggest a method, together with a computer code,³⁵ which eliminates these problems. The method is based on complementing a lattice unit cell with point charges, which zero out *all multipole moments* of the cell up to any predefined \mathcal{M} (see Figure 1b). If $\mathcal{M} \geq 2$, the potential in the inner region of the nanocluster converges absolutely to the result of the Ewald summation as the size of the nanocluster increases.³⁶ The complementary charges inside the nanocluster cancel each other out exactly by construction. Nonzero charges are situated only on the periphery of the nanocluster in a “skin” layer, thickness of which depends on the value of \mathcal{M} . Thus, the complementary charges provide corrective contribution to the EP inside the nanocluster without modifying the lattice structure in its inner region. This construction is convenient for embedded cluster calculations of crystalline systems and can be used to model bulk, surface, and low-dimensional structures.

Existing methods for constructing electrostatic embedding potential can be broadly divided into three categories:

Grouping. The crystal lattice can be divided into groups so as they have zero charge, dipole, and higher multipole moments.^{37,38} The potential produced by each of these groups is short range, and the sum over the groups converges absolutely if the first nonzero moment is octupole. For example, the lattice building blocks for the rock-salt and perovskite (Figure 2a and b, respectively) structures can be selected so as their first nonzero multipole moments are $m = 6$ and 4, respectively.

Fitting. The difference between the EPs produced by a finite system and the corresponding infinite solid is fitted

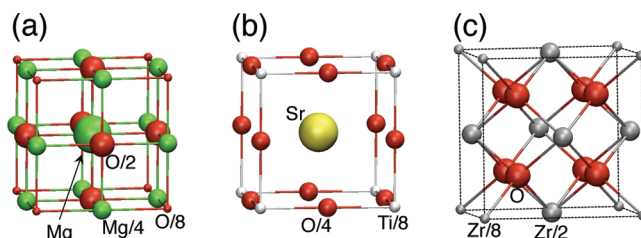


Figure 2. Examples of high-symmetry lattice building blocks: (a) $\text{MgO}:\text{Mg}(1/2\text{Mg})_{12}(1/2\text{O})_6(1/8\text{O})_8$; (b) $\text{SrTiO}_3:\text{Sr}(1/8\text{Ti})_8(1/4\text{O})_{12}$; (c) $\text{ZrO}_2:(1/2\text{Zr})_6(1/8\text{Zr})_8\text{O}_8$.

using a finite set of point charges.^{8,39–41} This usually involves three steps: (i) calculating the Madelung potential using the Ewald summation method; (ii) introducing discretization in order to define the number of fitting charges and their positions; and (iii) solving a system of linear equations to find the best fit.

Lattice Summation. The difference between the Madelung and EPs due to a finite cluster can be also reproduced using multipoles associated with the lattice ions⁴² or accounted for using the Ewald summation over infinite lattice.^{14,43}

An implicit limitation of the fitting and lattice summation approaches is in their reference to the infinite lattice model and the periodic boundary conditions, which makes them difficult to apply to, for example, nonperiodic systems and irregular surfaces. In addition, the procedures related to the charge discretization and to operating with differences between the Madelung potential and the potential produced by a finite cluster are user dependent. In particular, the accuracy of the potential can vary depending on the complexity of the system, size, and shape of the nanocluster and on the choice of the number and location of the fitting charges.

The method suggested here regularizes the *grouping* approach. It neither requires calculating the EP of an infinite system nor involves fitting. Moreover, the electrostatic embedding potential is reproduced by a finite set of point charges, which makes it easy to employ standard codes for ab initio calculations.

2. Regularization of the Electrostatic Potential Series

Consider a crystalline lattice with lattice vectors $\mathbf{R}_k = k_1\mathbf{a}_1 + k_2\mathbf{a}_2 + k_3\mathbf{a}_3$, where $\mathbf{a}_1, \mathbf{a}_2$, and \mathbf{a}_3 are elementary translation vectors, and k_1, k_2 , and k_3 are integers. If the position and the net charge of a j th atom in the unit cell are defined as ρ_j and e_j , respectively, the EP for this lattice is given by the equation:

$$V(\mathbf{r}) = \sum_{kj} \frac{e_j}{|\mathbf{r} - \mathbf{R}_k - \rho_j|} \quad (1)$$

where index j runs through all atoms in the unit cell, and index k runs through all unit cells of the system. In the case of infinite periodic lattices, the result of this summation depends on the order in which it is carried out.

The sum in eq 1 is not absolutely convergent, which means that, according to the Riemann series theorem, it can be made

to converge to any desired value from $-\infty$ to $+\infty$ by a suitable rearrangement of the terms. Ewald⁴⁴ has proposed a summation procedure which regularizes eq 1 and transforms it into a sum of two absolutely converging series. This regularization is achieved by interchanging an integration and an infinite summation, which does not converge uniformly (see, for example, ref 45). Physical implication of this regularization are discussed elsewhere.³⁸

An alternative approach, suggested by Madelung,⁴⁶ is based on regrouping the terms in eq 1:

$$V(\mathbf{r}) = \sum_k U(\mathbf{r} - \mathbf{R}_k) = \sum_k \left(\sum_{j=1}^N \frac{e_j}{|\mathbf{r} - \mathbf{R}_k - \rho_j|} \right) \quad (2)$$

where N is the number of centers in the group, so as the infinite sum over k becomes absolutely convergent. For this, it is necessary and sufficient to define the groups so as their zeroth, first, and second multipole moments, i.e., charge, dipole, and quadrupole, are all equal to zero simultaneously. The group of N centers does not have to coincide with the crystallographic unit cell but being translated with the corresponding lattice vectors should reproduce the whole infinite lattice.

Examples of such groups for MgO and SrTiO₃ are shown in Figure 2a and b, respectively. However, this method is difficult to generalize to complex lattices. It is straightforward to either select a unit cell or complement it with four fictitious charges,⁴⁷ so as to eliminate its dipole moment. However, eliminating the quadrupole and the higher electric moments in a general case is not trivial, and even in the case of cubic ZrO₂, the structural element shown in Figure 2c has nonzero components of the quadrupole moment.⁴⁸

In the following, we consider a crystal unit cell which, being translated along its vectors, fills up the lattice without voids and overlaps. We demonstrate that for any, however complex, crystal such a cell can be complemented with a set of point charges so as: (i) all of its electric moments up to and including any finite M are eliminated simultaneously, and (ii) being translated with all possible lattice translation vectors, the modified unit cell reproduces the original lattice. The EP inside a finite system, formed of these groups, converges with the size of the system absolutely if $M \geq 2$ and if the rate of the convergence is controlled by few well-defined numerical parameters.

Components of the m th multipole moment of a crystalline cell are defined as

$$Q_0(m_1, m_2, m_3) = \sum_{j=1}^{N_0} e_j \rho_{jx}^{m_1} \rho_{jy}^{m_2} \rho_{jz}^{m_3} \quad (3)$$

where N_0 is the number of atoms in the cell, and $m_1 + m_2 + m_3 = m$. For each m , sets (m_1, m_2, m_3) can be represented as points with integer coordinates in the first octangle, as shown in Figure 3a.³⁶ The zero moment component $Q_0(0, 0, 0)$, i.e., the unit cell charge, corresponds to the point at the origin in Figure 3b. Components $Q_0(1, 0, 0)$, $Q_0(0, 1, 0)$, and $Q_0(0, 0, 1)$ of the first moment, i.e., the unit cell dipole, correspond to the three points shown in Figure 3c. Points corresponding

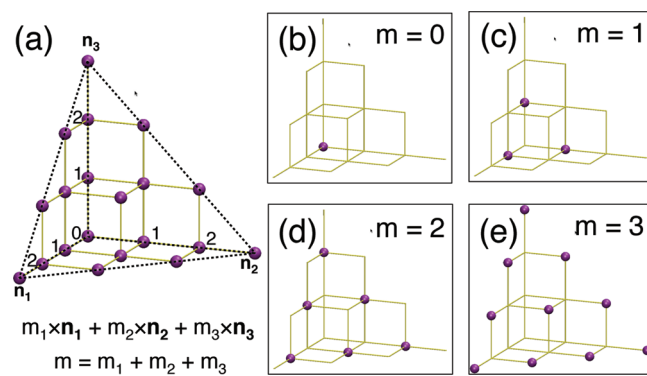


Figure 3. Correspondence between points occupying sites with integer coordinates m_1 , m_2 , and m_3 and components of multipole moments $x^{m_1}y^{m_2}z^{m_3}$, where the moment m is given by $m_1 + m_2 + m_3$.

to components of the quadrupole ($m = 2$) and octupole ($m = 3$) moments are shown in Figure 3 d and e, respectively.

In general, all components of all multipole moments up to $m = M$ can be associated with integer-coordinate points inside a tetrahedron T_M with vertices at $(0, 0, 0)$, $(M, 0, 0)$, $(0, M, 0)$, and $(0, 0, M)$.³⁶ Such tetrahedron for $M = 3$ is shown with dashed lines in Figure 3a. For convenience, point $(0,0,0)$ will be referred to as the main vertex of the tetrahedron.

We exploit this correspondence so as to eliminate multipole moments of the original unit cell. For that we introduce a set of point charges $e(\mathbf{n})$ at

$$\rho(\mathbf{n}) = n_1 \mathbf{a}_1 + n_2 \mathbf{a}_2 + n_3 \mathbf{a}_3, \quad \mathbf{n} \in T_M \quad (4)$$

where $\mathbf{n} = (n_1, n_2, n_3)$. Since the tetrahedron defined for components of multipole moments and the tetrahedron defined for charges $e(\mathbf{n})$ are equivalent, it is always possible to obtain such values of $e(\mathbf{n})$ that the multipole moments due to these charges cancel out the multipole moments of the original unit cell exactly:

$$\sum_{\mathbf{n} \in T_M} e(\mathbf{n}) \rho_x^{m_1}(\mathbf{n}) \rho_y^{m_2}(\mathbf{n}) \rho_z^{m_3}(\mathbf{n}) = -Q_0(\mathbf{m}), \quad \mathbf{m} \in T_M \quad (5)$$

In principle, this system of linear equations can be solved with respect to $e(\mathbf{n})$ using standard matrix diagonalization algorithms. However, the matrix elements can vary by several orders of magnitude, resulting in the loss of accuracy of the numerical solutions.

A general method for solving this system of equations analytically has been proposed in ref 36. Here we generalize this method in order to account for the fact that the EP function in a system has the same symmetry as the system itself. To this end, the tetrahedra T_M^α ($\alpha = 1, 2, \dots, 8$) and the corresponding set of extra charges are associated with each corner of the lattice unit cell.

For convenience, we will use fractional coordinates and assume that the corners of the unit cell are at the points $(\mp 1/2, \mp 1/2, \mp 1/2)$, where each combination of signs defines one of the corners and corresponds to one of the values of α . Then, positions of the main vertices of the tetrahedra T_M^α are given by

$$\mathbf{r}_0^\alpha = \mp\left(\frac{1}{2} + \nu\right)\mathbf{a}_1 \mp \left(\frac{1}{2} + \nu\right)\mathbf{a}_2 \mp \left(\frac{1}{2} + \nu\right)\mathbf{a}_3 \quad (6)$$

where parameter ν defines the shift of T_M^α with respect to the corresponding corner of the unit cell, and the charges $e^\alpha(\mathbf{n})$ are positioned at (compare with eq 4)

$$\rho^\alpha(\mathbf{n}) = \mathbf{r}_0^\alpha \pm n_1\mathbf{a}_1 \pm n_2\mathbf{a}_2 \pm n_3\mathbf{a}_3 \quad (7)$$

The values of charges $e^\alpha(\mathbf{n})$ for each of the tetrahedra can be calculated separately in order to eliminate a fraction of the multipole moments of the original unit cell. For simplicity, for each α we choose, the coordinate system in which $\mathbf{r}_0^\alpha = 0$, and require that the extra charges associated with a tetrahedron T_M^α cancel 1/8th of the unit cell multipole moments, i.e., $P^\alpha(\mathbf{m}) = (1/8)P_0(\mathbf{m})$, where $P_0(\mathbf{m})$ defines multipole moments of the original unit cell calculated in the same coordinate system and expressed in fractional coordinates. Then, eq 5 becomes

$$\sum_{\mathbf{n} \in T_M^\alpha} e^\alpha(\mathbf{n})(\pm n_1)^{m_1}(\pm n_2)^{m_2}(\pm n_3)^{m_3} = -P^\alpha(\mathbf{m}), \quad \mathbf{m} \in T_M^\alpha \quad (8)$$

where the signs are defined by the orientation of T_M^α and are opposite to those in eq 6.

This system of equations can be solved analytically with the help of auxiliary functions:³⁶

$$G_k(x) = \begin{cases} 0 & \text{if } k = 0 \\ \prod_{j=0}^{k-1} (x - j) & \text{if } k > 0 \end{cases} \quad (9)$$

which, for integer values of the argument, become

$$G_k(n) = \begin{cases} 0 & \text{if } n < k \\ \frac{n!}{(n - k)!} & \text{if } n \geq k \end{cases} \quad (10)$$

Functions $G_k(x)$ are polynomials of x :

$$G_k(x) = \sum_{m=0}^k g(k, m)x^m \quad (11)$$

and their coefficients $g(k, m)$ can be calculated analytically using recurrence equations:

$$\begin{aligned} g(k+1, 0) &= kg(k, 0) = g(1, 0) = 0 \\ g(k+1, k+1) &= g(k, k) = g(0, 0) = 1 \\ g(k+1, m) &= g(k, m-1) - kg(k, m), \quad m = 1, \dots, k \end{aligned} \quad (12)$$

In one-dimensional case, the system of eqs 8 transforms into

$$\sum_{n=0}^M (\pm n)^m e^\pm(n) = -P^\pm(m), \quad m = 0, 1, \dots, M \quad (13)$$

where we adopted the \pm sign instead of α ($\alpha = 1, 2$). Multiplying these equations by $(\pm 1)^m g(k, m)$ and summing over m we obtain

$$\sum_{m=0}^k \sum_{n=0}^M g(k, m)n^m e^\pm(n) = - \sum_{m=0}^k (\pm 1)^m g(k, m)P^\pm(m) \quad (14)$$

where $k = 0, \dots, M$. The right side of this equation is known and, for brevity, is denoted as $f^\pm(k)$, while the left side contains the expansion of $G_k(n)$ over powers of n :

$$\sum_{n=0}^M G_k(n)e^\pm(n) = f^\pm(k), \quad k = 0, \dots, M \quad (15)$$

Taking into account the properties of $G_k(n)$ (see eq 10), we obtain backward relations for the charges $e(n)$:

$$e^\pm(M) = \frac{1}{M!}f^\pm(M) \quad (16)$$

and

$$e^\pm(k) = \frac{1}{k!} \left(f^\pm(k) - \sum_{n=k+1}^M \frac{n!}{(n-k)!} e^\pm(n) \right) \quad (17)$$

where $k = M-1, M-2, \dots, 0$.

Similar, although more complex, backward recurrence relations can be obtained for the three-dimensional case³⁶ and for any tetrahedron T_M^α . For simplicity, we omit the explicit index α , since the reference to each tetrahedron is incorporated in the choice of signs for $(\pm 1)^{m_i}$ ($i = 1, 2, 3$) in eq 8 and the values of the multipole moments $P(\mathbf{m})$, calculated in the coordinate system selected for each tetrahedron, as described above.

We reenumerate points (k_1, k_2, k_3) of a tetrahedron T_M from 1 to N_M , using a single index $k = \varphi(k_1, k_2, k_3)$ and the explicit relation (see ref 36 for details):

$$k = \varphi(k_1, k_2, k_3) =$$

$$\begin{aligned} &\frac{1}{6}k_1[3M^2 + 12M + 11 - 3(M+2)k_1 + k_1^2] \\ &+ k_2(M+1-k_1) - \frac{1}{2}k_2(k_2-1) + k_3 + 1 \end{aligned} \quad (18)$$

In this numeration, the first index $k = 1$ corresponds to the point (0,0,0) and the last index $k = N_M$ corresponds to the point (M,0,0) of the tetrahedron.

Using the single index numeration, we introduce functions:

$$\tilde{e}(n) = e(n_1, n_2, n_3)$$

$$\tilde{G}_k(n) = G_{k_1}(n_1)G_{k_2}(n_2)G_{k_3}(n_3)$$

and

$$\tilde{f}(k) = f^{\pm\pm\pm}(k_1, k_2, k_3) \quad (19)$$

where $\tilde{f}(k)$ is known

$$\begin{aligned} \tilde{f}(k) = - \sum_{m_1=0}^{k_1} \sum_{m_2=0}^{k_2} \sum_{m_3=0}^{k_3} P^\alpha(\mathbf{m}) &(\pm 1)^{m_1}(\pm 1)^{m_2}(\pm 1)^{m_3} \\ &\times g(k_1, m_1)g(k_2, m_2)g(k_3, m_3) \end{aligned} \quad (20)$$

and the choice of signs is defined by that in eq 8. Then, the recurrent relations analogous to eqs 16 and 17 can be written as

$$\tilde{e}(N_M) = \frac{1}{\tilde{G}_{N+M}(N_M)}\tilde{f}(N_M)$$

$$\tilde{e}(k) = \frac{1}{\tilde{G}_k(k)} \left(\tilde{f}(k) - \sum_{n=k+1}^{N_{\mathcal{M}}} \tilde{G}_k(n) \tilde{e}(n) \right) \quad (21)$$

where $k = N_{\mathcal{M}} - 1, N_{\mathcal{M}} - 2, \dots, 0$, and

$$\tilde{G}_k(n) = \frac{n_1!}{(n_1 - k_1)!} \frac{n_2!}{(n_2 - k_2)!} \frac{n_3!}{(n_3 - k_3)!}, \quad k \leq n \quad (22)$$

We note that for nanoclusters with characteristic size of more than $2\mathcal{M}$ unit cells, there is a finite inner region in which all charges $e(\mathbf{n})$ belonging to the same tetrahedron $T_{\mathcal{M}}$ will occupy the same lattice site exactly once. Since the sum of such complementary charges is zero for neutral cells (see eq 5), these charges cancel each other out. Hence, nonzero complementary charges remain only on the periphery of the nanocluster.

3. Details of the Calculations

In the following, we apply the method described in Section 2 to several crystalline lattices. In each case, a lattice unit cell is complemented with a set of charges $e(\mathbf{n})$ so as to eliminate several of its multipole moments. These modified unit cells are used to generate a series of finite systems (see Figure 4) as their

$$(2k_1k + 1) \times (2k_2k + 1) \times (2k_3k + 1) \quad k = 0, 1, 2, \dots \quad (23)$$

extensions, i.e., a finite system is constructed by repeating the lattice building block $(2k_1k + 1)$, $(2k_2k + 1)$, and $(2k_3k + 1)$ times along the lattice vectors \mathbf{a}_1 , \mathbf{a}_2 , and \mathbf{a}_3 , respectively. Thus, parameters k_1 , k_2 , and k_3 define the shape of the cluster, and parameter k defines its size.

The convergence of the EP is investigated as a function of the system size and shape, the largest eliminated multipole moment \mathcal{M} , the number of tetrahedra $T_{\mathcal{M}}$, and the values of the shift parameter v .

To assess the convergence of the EP, we calculate the potential produced by all centers of the system at the atom

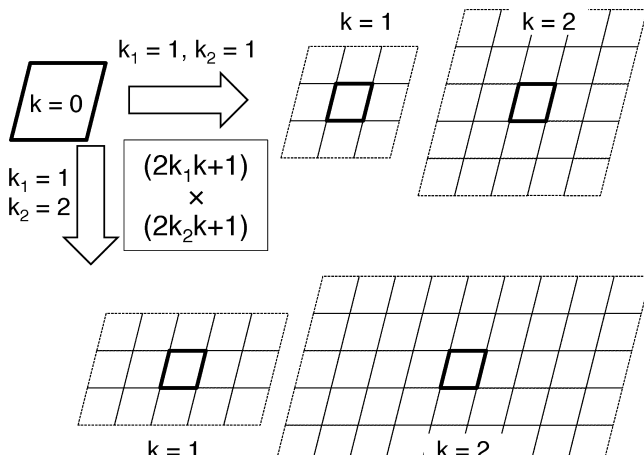


Figure 4. Schematics of the finite clusters constructed according to the $(2k_1k + 1) \times (2k_2k + 1)$ rule for $k_1 = k_2 = 1$ (top) and $k_1 = 1$ and $k_2 = 2$ (bottom). The central unit cell is shown with bold lines.

sites of the central unit cell, i.e., the *on-site* potential (V^{site}) and the potential in the space *between* the atoms, which is calculated on a three-dimensional grid (V^{grid}) in the central unit cell. In this work, we used a regular grid of 21^3 points, from which we removed the points if they are within 0.6 Å of any lattice atom. Thus, the total number of remaining grid points was close to 8000.

To characterize convergence of the EP, we consider deviations from the reference potential calculated using the Ewald method (V^{Ewald}) for each point i

$$\Delta V_i = V_i^{\text{Ewald}} - V_i \quad (24)$$

and the root-mean-square (rms) and the standard deviation of ΔV_i :

$$\Delta V_{\text{rms}} = \sqrt{\frac{1}{N} \sum_i^N (\Delta V_i)^2} \quad (25)$$

$$\sigma = \sqrt{\frac{1}{N} \sum_i^N (\Delta V_i - \bar{\Delta V})^2} \quad (26)$$

where

$$\bar{\Delta V} = \sum_i^N \Delta V_i \quad (27)$$

is the mean of ΔV_i , and index i runs through all atoms of the central unit cell in the case of the on-site potential ($V = V^{\text{site}}$) and through all grid points in the case of the potential calculated on the grid ($V = V^{\text{grid}}$).

Structural parameters of the materials selected for this study are summarized in Table 1. The first group includes binary oxides in which the unit cell period is comparable to the interatomic distances: rock-salt MgO, rutile TiO₂, and α -quartz SiO₂. Due to the high symmetry of the rock-salt lattice, the unit cell used for MgO has zero dipole and quadrupole moments. In the case of rutile, only one component of the dipole moment and three components of the quadrupole moment are equal to zero.

The second group of materials includes complex oxides with ~ 50 –100 atoms per cell and with a lattice period significantly larger than typical interatomic distances. The EP function in these materials has a complex character combining potential variations on the scale of cation–anion distances with longer range variations on the scale of the lattice period.

4. Results

In this section we will investigate the convergence of the EP inside finite systems constructed of building blocks, for which the first \mathcal{M} electric multipole moments are exactly zero. In Section 4.1, we demonstrate that if $\mathcal{M} < 2$, then the EP depends on the shape of the finite systems and illustrate how the absolute convergence of the EP can be achieved using larger \mathcal{M} . The dependence of the EP on the parameter v (see eq 6) is discussed in Section 4.2. In Section 4.3, we demonstrate that using charges $e(\mathbf{n})$ of eight tetrahedra T^a can improve the EP convergence. Finally, in Section 4.4,

Table 1. Crystal Lattices Considered in This Work^a

material	structure	cell parameters				
		<i>a</i>	<i>b</i>	<i>c</i>	α	β
MgO	rock-salt	4.0	4.0	4.0	90.0	90.0
TiO ₂	rutile	4.59373	4.59373	2.95812	90.0	90.0
SiO ₂	α -quartz	4.91304	4.91304	5.40463	90.0	90.0
Ba ₄ Fe ₈ Si ₈ O ₂₈	andremeyerite	7.464	13.794	7.093	90.0	118.25
Na ₇ [Al ₄ Si ₁₂]Si ₈ O ₄₈ Cl ₃	marielite	12.047	12.047	7.5602	90.0	90.0
Na ₁₆ Ce ₈ [CO ₃] ₂₀	petersenite (Ce)	20.872	6.367	10.601	90.0	120.5

^a Structural parameters *a*, *b*, *c* (in Å) and α , β , γ (in degrees) are given according to the crystallographic convention.

we investigate the EP convergence in the lattices of minerals, which have large unit cells and complex character of the EP function.

4.1. Size- and Shape-Dependence of The EP. To illustrate the dependence of the EP inside a finite system on the shape and the size of this system, we applied the $(2k_1k+1) \times (2k_2k+1) \times (2k_3k+1)$ rule, schematically illustrated in Figure 4, to construct a series of rutile TiO₂ clusters. We note that for a fixed set of numbers k_i ($k_i \geq 1$, $i = 1, 2, 3$) increasing parameter *k* to infinity corresponds to the summation over the infinite lattice, while parameters k_1 , k_2 , and k_3 define a particular order of this summation.

In this set of the calculations, we used eight tetrahedra $T_{\mathcal{M}}$ and fixed the value of the parameter *v* (see eq 6) to *v* = 0.5. We considered three sets of k_1 , k_2 , and k_3 :

$$\begin{aligned} k_1 &= 1, \quad k_2 = 1, \quad k_3 = 1 \\ k_1 &= 1, \quad k_2 = 1, \quad k_3 = 2 \\ k_1 &= 1, \quad k_2 = 2, \quad k_3 = 2 \end{aligned}$$

and varied parameter *k* from 1 to 5. The dependence of $\Delta V_{\text{rms}}^{\text{site}}$ on *k* and k_i , calculated for several different \mathcal{M} , is shown in Figure 5.

We emphasize that the original rutile TiO₂ unit cell has two nonzero components of the dipole moment [$Q(0, 1, 0) = Q(0, 0, 1) = -9.2 \text{ e}\text{\AA}$] and three nonzero components of the quadrupole moment [$Q(0, 2, 0) = Q(2, 0, 0) = -32.2 \text{ e}\text{\AA}^2$, $Q(1, 1, 0) = -16.4 \text{ e}\text{\AA}^2$]. The procedure described in

Section 2 was used to complement the original unit cell with point charges and, thus, to generate rutile TiO₂ lattice building blocks, which have no nonzero multipole moments up to $\mathcal{M} = 4$.

The results shown in Figure 5a demonstrate that for $\mathcal{M} = 0$, the $\Delta V_{\text{rms}}^{\text{site}}$ converges to a constant value with an increasing value of *k*. The corresponding standard deviation σ^{site} (eq 26) also converges to a constant and nonzero value. For example, for $k = 5$, $\sigma^{\text{site}} = 13.3 \text{ V}$, if $k_1 = k_2 = k_3 = 1$, $\sigma^{\text{site}} = 19.7 \text{ V}$, if $k_1 = k_2 = 1$ and $k_3 = 2$, and $\sigma^{\text{site}} = 18.5 \text{ V}$, if $k_1 = 1$ and $k_2 = k_3 = 2$. In other words, the difference between V^{site} and V^{Ewald} varies from site to site and cannot be improved by further increasing *k*. In addition, the convergence limit depends on the choice of k_i , i.e., the potential distribution inside the finite cluster is determined by its shape even in the case of an infinitely large *k*. This is characteristic to a series in which the result of the summation depends on the order of this summation, which, in our case, is defined by the parameters k_i .

If the original unit cell is complemented with extra charges so as its dipole, but not quadrupole, moment becomes zero ($\mathcal{M} = 1$), the EP still depends on the order of the summation, as demonstrated in Figure 5b. Indeed, series $\sim 1/r^3$ diverges as $\ln(R)$ when summed up over a sphere of radius *R*. In practice, convergence is achieved by fixing the order of the summation. In the case of TiO₂ (see Figure 5b), we found that dispersion σ^{site} tends to zero as the value of *k* is increased, i.e., the EP in the finite system differs from the corresponding V^{Ewald} by a constant value. We emphasize that the numerical value of that shift is defined entirely by the parameters k_i (*i* = 1, 2, 3) and, in general, by the shape of the finite system.

Once the unit cell is modified so as its quadrupole moment is eliminated ($\mathcal{M} = 2$), the EP converges to V^{Ewald} with increasing *k* absolutely, as illustrated in Figure 5c. The speed of the convergence still depends on the parameters k_i , i.e., on the shape of the finite system. Similar results, but faster convergence rates, were obtained for $\mathcal{M} = 3$ and 4 (Figure 5d–e).

4.2. Dependence on the Shift Parameter *v*. The method described in Section 2 leaves one free to choose the value of the parameter *v*, which defines the shift of the tetrahedra $T_{\mathcal{M}}$ from their respective corners of the unit cell. Hence, this parameter can be varied in order to minimize the number of the charges and ΔV_{rms} for a given value of \mathcal{M} and to improve the convergence of the EP.

The maximum number of charges $e(\mathbf{n})$ associated with each tetrahedron is defined by the value of \mathcal{M} as $n_q = (\mathcal{M} + 1)(\mathcal{M} + 2)(\mathcal{M} + 3)/6$. Hence, the maximum total number

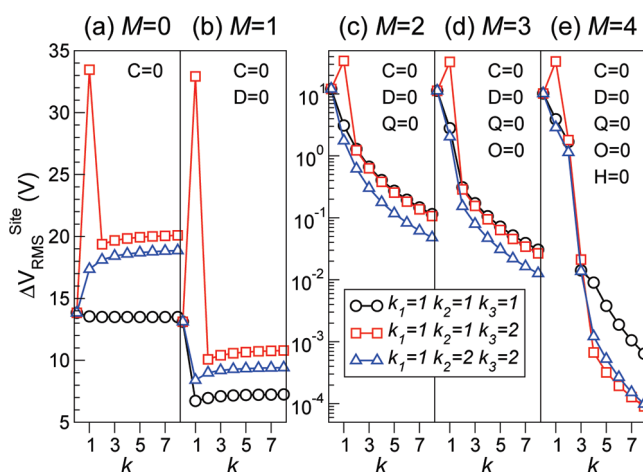


Figure 5. Convergence of the on-site EP calculated for the central unit cell of $(2k_1k+1) \times (2k_2k+1) \times (2k_3k+1)$ rutile TiO₂ clusters. \mathcal{M} is the largest eliminated electric moment. Letters *C*, *D*, *Q*, *O*, and *H* refer to the charge, dipole, quadrupole, octopole, and hexadecapole moments of the modified unit cell, respectively.

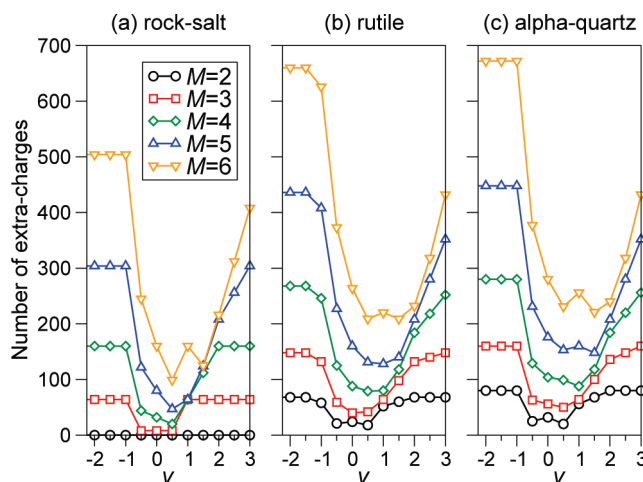


Figure 6. The total number of complementary charges $e(\mathbf{n})$ associated with $T_{\mathcal{M}}^{\alpha}$ ($\alpha = 1, \dots, 8$) calculated for the unit cells of rock-salt, rutile, and α -quartz lattices and plotted as a function of the shift parameter v .

of the charges is given by the number of tetrahedra used multiplied by n_q .

However, for all integer and half-integer values of v some of the charges, belonging to different tetrahedra, coincide and may cancel each other out due to the lattice symmetry. For illustration, we plot the total number of charges, N_q , for rock-salt, rutile, and α -quartz lattices and several values of \mathcal{M} in Figure 6. Eight tetrahedra were used in each case, which gives the maximum total number of charges $8n_q = 80$ for $\mathcal{M} = 2$, 160 for $\mathcal{M} = 3$, and 280 for $\mathcal{M} = 4$.

As it is clear from Figure 6, the number of charges N_q is considerably smaller than $8n_q$ for the highly symmetrical rock-salt lattice (Figure 6a) but not so for lower symmetry rutile and α -quartz (Figure 6b and c, respectively). This is because many components of the electric multipole moments are equal to zero in the rock-salt structure, which translates into zero values of many of the charges $e(\mathbf{n})$.

For $v \geq -0.5$, positions of some of the charges $e^{\alpha}(\mathbf{n})$ belonging to different $T_{\mathcal{M}}^{\alpha}$ coincide, and their values can cancel each other out exactly. Consequently, the number of these charges can decrease by as much as a factor of 3 in α -quartz and by a factor of 5 in rock-salt lattices.⁴⁹

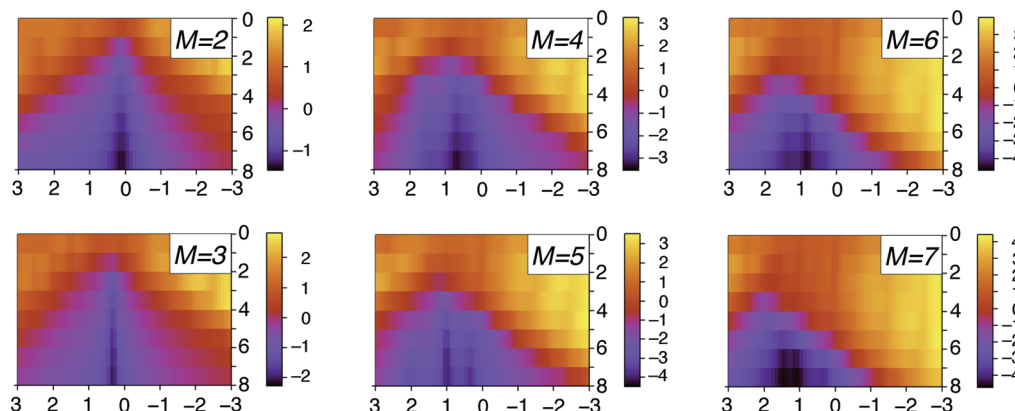


Figure 7. Convergence of $\Delta V_{\text{rms}}^{\text{grid}}$ in rutile TiO_2 calculated for several values of \mathcal{M} and the shift parameter v : $-3 \leq v \leq 3$. Darker regions indicate smaller values of $\Delta V_{\text{rms}}^{\text{grid}}$; the corresponding range of values is shown on the right of each plot using a \log_{10} scale.

The dependence of $\Delta V_{\text{rms}}^{\text{grid}}$ on the shift parameter v and the size parameter k calculated for rutile TiO_2 is shown in Figure 7. Here the value of v was varied from -3 to $+3$ with increments of 0.1 , and the value of k was varied from 0 to 8 .

It is clear that for all v and any \mathcal{M} ($\mathcal{M} \geq 2$), the function $\Delta V_{\text{rms}}^{\text{site}}(v, k)$ converges to zero in the limit of large k . For $\mathcal{M} = 2$ and 3 , this function has a narrow deep valley, indicating that the convergence of the EP can be significantly improved by choosing an appropriate v . Interestingly, for $\mathcal{M} = 4-7$, we obtain a relatively wide valley, where $\Delta V_{\text{rms}}^{\text{site}}(v, k)$ is small and almost independent of v . This suggests that for large values of \mathcal{M} , the EP, due to the modified unit cell, is short range. Hence, the EP inside a finite system converges with its size, as defined by k , quickly. At the same time, geometrical size of each $T_{\mathcal{M}}^{\alpha}$ becomes large compared to the size of the original unit cell, which makes the results less dependent on the details of their relative geometrical arrangement, as given by v . Interestingly, the range of v providing fast convergence of the EP coincides with that for which N_q is the smallest.

To summarize, parameter v determines the shift of the extra charges from the unit cell corners and serves two purposes. First, the total number of extra charges can be reduced significantly if $v > 0$, as illustrated in Figure 6. Second, positive v can improve convergence of the electrostatic with respect to the highest eliminated multipole moment and the size of the nanocluster (Figure 7). In addition, parameter v offers flexibility in positioning the extra charges, with respect to the atomic coordinates, which may be of an advantage in modeling surface sites.

4.3. Dependence on Spatial Distribution of the Charges $e(\mathbf{n})$.

The charges $e^{\alpha}(\mathbf{n})$ associated with any single tetrahedron $T_{\mathcal{M}}^{\alpha}$ are sufficient to eliminate all electric moments of the unit cell up to any predefined \mathcal{M} .³⁶

In this section, we investigate the effects of symmetrical spatial distribution of the charges $e(\mathbf{n})$ generated for several tetrahedra. For example, it can be expected that the charges associated with eight tetrahedra positioned symmetrically at the corners of the unit cell, as indicated in Figure 8c, could provide faster convergence of the EP than those due to a single tetrahedron (see Figure 8a).

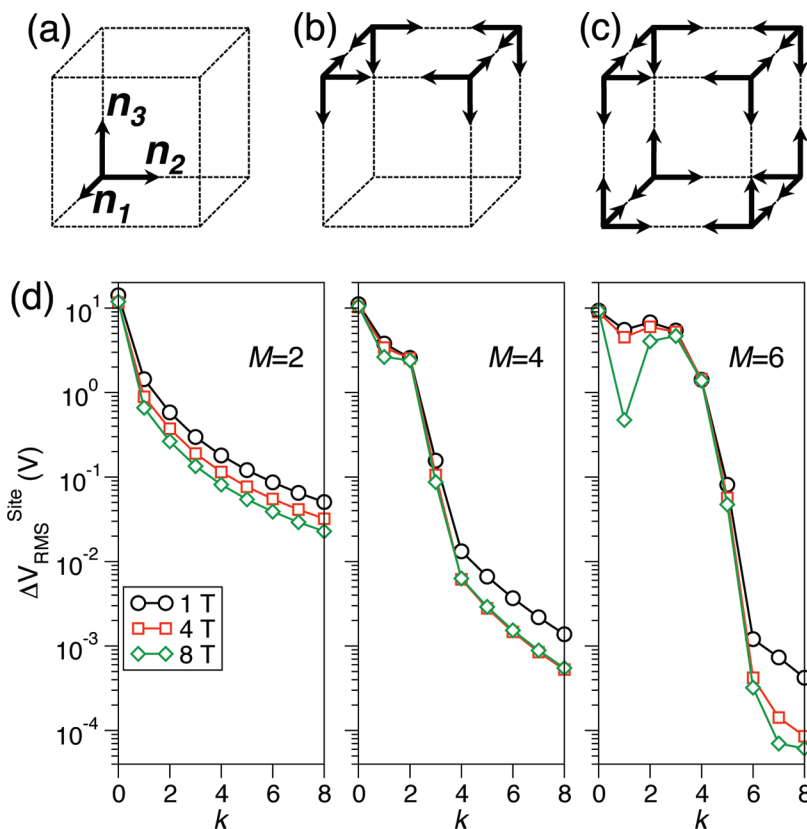


Figure 8. Convergence of the on-site EP in α -quartz. The values of $\Delta V_{\text{rms}}^{\text{site}}$ are calculated for clusters generated using eq 23 with $k_1 = k_2 = k_3 = 1$. The charges are generated using one (1 T), four (4 T) and eight (8 T) tetrahedra as indicated in a, b, and c, respectively. The orientation of each tetrahedron is given by vectors \mathbf{n}_1 , \mathbf{n}_2 , and \mathbf{n}_3 , which are collinear with the lattice vectors \mathbf{a}_1 , \mathbf{a}_2 , and \mathbf{a}_3 (not shown) of the unit cell, indicated with a dashed box in a–c. \mathcal{M} shows the value of the largest eliminated multipole.

We consider the α -quartz SiO_2 lattice and construct the charges $e(\mathbf{n})$ using one, four, and eight tetrahedra as indicated in Figure 8, in order to eliminate the electric moments up to $\mathcal{M} = 2, 4$, and 6 in each case. A series of finite clusters was constructed using the $(2k+1)^3$ rule, given by eq 23 with $k_1 = k_2 = k_3 = 1$, for $k = 0, 1, \dots, 8$, and the values of $\Delta V_{\text{rms}}^{\text{site}}$ were calculated for the central cell of each cluster. The results of these calculations for the shift vector $v = 0.0$ are plotted in Figure 8d.

It is clear that even in the case of the low-symmetry lattice, such as that of α -quartz, the convergence of the EP can be improved if several T_M^α tetrahedra of charges are used. We note that, in this particular case, the $e(\mathbf{n})$ constructed for the four and eight tetrahedra demonstrate almost identical behavior of $\Delta V_{\text{rms}}^{\text{site}}$ with the value of k .

The advantages of using eight symmetrically located tetrahedra becomes apparent if we consider the dependence of $\Delta V_{\text{rms}}^{\text{site}}$ on the shift vector v , as shown in Figure 9. Here we plot $\Delta V_{\text{rms}}^{\text{site}}$ as a function of v for three sizes of the α -quartz clusters ($k = 4, 6, 8$) and $\mathcal{M} = 4$ and 6.

In the case of a single tetrahedron, $\Delta V_{\text{rms}}^{\text{site}}$ strongly depends on v , i.e., achieving good EP convergence requires pre-optimization of the shift parameter. The dependence on the value of v is less pronounced in the case of four tetrahedra. Finally, if eight tetrahedra are used, the $\Delta V_{\text{rms}}^{\text{site}}$ shows small variations near its minimum, which is broadly in the region of $0 \leq v \leq 1$.

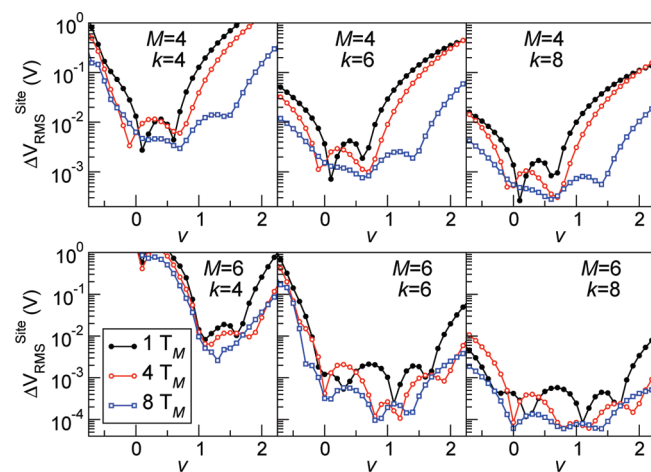


Figure 9. Dependence of $\Delta V_{\text{rms}}^{\text{site}}$ in the central cell of α -quartz clusters on the shift parameter v . Complementary charges $e(\mathbf{n})$ are generated using one (closed circles), four (open circles), and eight (open squares) tetrahedra T_M for $\mathcal{M} = 4$ (top panels) and 6 (bottom panels). The clusters are generated using eq 23 with $k_1 = k_2 = k_3 = 1$.

This observation is consistent with the results obtained for $\Delta V_{\text{rms}}^{\text{grid}}$ in rutile TiO_2 (Section 4.2) and suggests that the particular choice of v is insignificant for $\mathcal{M} \geq 4$ and $k \geq 4$ as long as $0 \leq v \leq 1$.

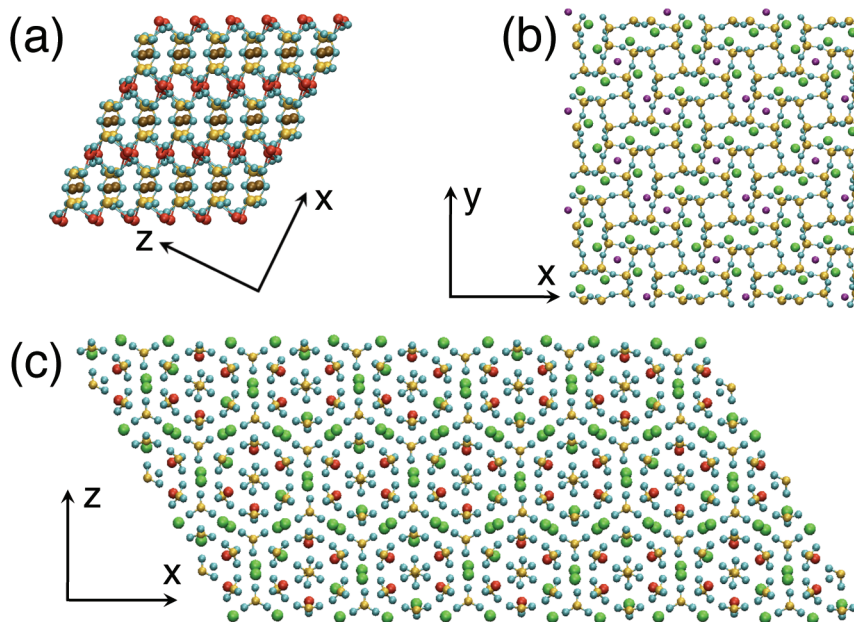


Figure 10. Structure of complex oxides used in this work: (a) andremeyerite $\text{Ba}_4\text{Fe}_8\text{Si}_8\text{O}_{28}$; (b) marialite $\text{Na}_7[\text{Al}_4\text{Si}_{12}]\text{Si}_8\text{O}_{48}\text{Cl}_3$, and (c) petersenite $\text{Na}_{16}\text{Ce}_8[\text{CO}_3]_{20}$. Each panel shows a $(2k + 1)^3$ extension of the corresponding unit cell with $k = 1$. Structural parameters of these systems are given in Table 1.

4.4. Electrostatic Potential in Complex Lattices. To illustrate the applicability of the method to a wide range of systems, we considered three minerals having complex lattice structures formed by several types of atoms with different formal ionic charges (see Table 1 and Figure 10).

In particular, andremeyerite has a monoclinic lattice and 48 ions per cell with formal charges of -2 , $+2$, and $+4$. Marialite has tetragonal lattice, and its unit cell contains 82 ions with the charges of -2 , -1 , $+1$, $+3$, and $+4$. Finally, petersenite has a monoclinic lattice and contains 20 molecular anions CO_3 per cell. These anions were modeled using the corresponding formal charges as $\text{C}^{4+}\text{O}_3^{2-}$ anions, which provide strong variations of the EP on the scale of the interatomic distances.

The EP distribution in these systems is further complicated by the long-range modulations on the scale of the lattice period and by large differences in the values of the crystallographic parameters. For example, in petersenite, the value of the lattice parameter a is $\sim 20.872 \text{ \AA}$ and the ratios a/b and a/c are ~ 3.2 and ~ 2.0 , respectively.

In each case, we have modified the initial unit cell in order to eliminate \mathcal{M} lowest multipole moments and used these modified cells to generate finite $(2k + 1)^3$ systems, as described above. Convergence of the EP was investigated as a function of the system size. In all cases, we used eight T^0 tetrahedra, and the value of the shift parameter v was fixed to zero. The results of these calculations are collected in Figure 11.

The calculated function $\Delta V_{\text{rms}}^{\text{site}}(k, \mathcal{M})$ does not generally approach zero if the cell is neutral and has no dipole moment, simultaneously, i.e., $\mathcal{M} = 1$. Instead, $\Delta V_{\text{rms}}^{\text{site}}$ converges to a constant value, as it is shown in Figure 11a–c, which depends on the order of summation, as discussed above in Section 4.1 on the example of rutile TiO_2 . The convergence becomes absolute if the quadrupole moment is eliminated as well, i.e., $\mathcal{M} \geq 2$.

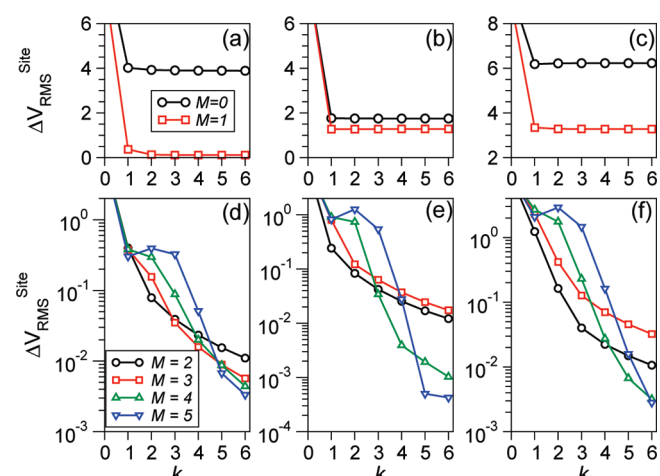


Figure 11. Convergence of the on-site EP in andremeyerite (a, d), marialite (b, e), and petersenite (c, f) clusters generated using eq 23 with $k_1 = k_2 = k_3 = 1$. The original unit cells have been modified to eliminate all electric moments up to and including \mathcal{M} . In the case of unit cells with nonzero quadrupole ($\mathcal{M} < 2$), the potential converges to an arbitrary limit defined by the shape of the cluster (a–c). The absolute convergence is achieved if $\mathcal{M} \geq 2$ (d–e).

The convergence with respect to the system size is faster for larger values of \mathcal{M} , as illustrated in Figure 11d–f. We notice that, in some cases, functions $\Delta V_{\text{rms}}^{\text{site}}(k, \mathcal{M})$ calculated for an even $\mathcal{M} = \mathcal{M}_1$ and odd $\mathcal{M} = \mathcal{M}_1 + 1$ behave similarly with k . This can be seen for both marialite and petersenite for $\mathcal{M} = 2$ and 3 and for $\mathcal{M} = 4$ and 5. This is because in the case of even \mathcal{M} some components of the higher electric moments can become eliminated by symmetry, and hence, further increase of \mathcal{M} by 1 may improve the convergence insignificantly.

The overall convergence of the EP in the considered minerals is similar to that found for simpler structures, such

as rutile and α -quartz. Similarly good convergence was found for the EP calculated on the grid and characterized using $\Delta V_{\text{rms}}^{\text{grid}}(k, \mathcal{M})$.

5. Discussion and Conclusions

The relation between the electrostatic potential (EP) inside a finite macroscopic sample and its surface charge as well as the dependence of the potential on the shape of the sample have been considered previously in, for example, refs 50–52. It is well-known that surfaces of macroscopic samples acquire surface charge in order to compensate the EP *outside* the sample. There can be several sources of the surface charge, including surface reconstruction, contamination with impurities, and defect formation, all of which can be difficult to describe on the atomic scale.

In our method, the lattice unit cell is complemented with charges $e(\mathbf{n})$ so as the EP produced by each modified cell is short range, which is the physical basis for the proposed regularization of eq 1. Indeed, the EP *outside* a finite system constructed from these unit cells is also short range independently on its size and shape, as expected for realistic macroscopic samples. It can also be said that charges $e(\mathbf{n})$ produce effective compensating potential, which does not need to be described on the atomic scale.

The potential *inside* a finite system converges with its size absolutely, and the rate of convergence is controlled by few numerical parameters: the largest eliminated multipole moment of the original unit cell \mathcal{M} , the number of the tetrahedra $T_{\mathcal{M}}$ of the complementary charges, and the displacement v of the main tetrahedra vertices with respect to the unit cell corners. We note that the absolute convergence of the EP with the size of the system is achieved only if $\mathcal{M} \geq 2$ and can be improved by increasing \mathcal{M} further, by using a symmetry adjusted number of tetrahedra and by varying the value of v . As demonstrated above, elimination of the unit cell dipole moment only ($\mathcal{M} = 1$) does not eliminate the dependence of the EP on the shape of the finite system. Importantly, as the size of the finite system increases, the EP inside of it converges to the result of the Ewald summation for the corresponding infinite lattice.³⁶ Thus, regularization of the Coulomb series proposed in our method is equivalent to that used in the Ewald method.

We note that nonzero complementary charges $e(\mathbf{n})$ are situated only near the periphery of the nanocluster, while in its inner region, the lattice remains unchanged. This property of $e(\mathbf{n})$, together with the rapid convergence of the EP with the size of the nanocluster, makes this method convenient to use in embedded cluster calculations of crystalline materials. This method can be also used for disordered materials and liquids as well as low-dimensional systems (surfaces, quasi-one-dimensional wires, and clusters), providing they can be represented using a supercell approach. Indeed, a supercell can be considered on the same footing as a conventional crystalline cell, and the same formalism can be applied. We can add that the supercell, complemented with the extra-charges $e(\mathbf{n})$, can be considered as a lattice building block and can be used to construct arbitrary finite structures consistent with the problem at hand.

The computational cost of generation charges $e(\mathbf{n})$ for a unit cell depends on the largest multipole moment to be eliminated and on the number of particles in the unit cell and scales as $\mathcal{M}^3 \mathcal{N}_0$. The unit cell complemented with the extra charges is used to construct a nanocluster of $(2k + 1)^3$ unit cells, which makes the total number of atoms in the system $N = (2k + 1)^3 \mathcal{N}_0$; the number of nonzero extra charges at the surface of the nanoclusters scales as $\mathcal{M}^3 k^2$. Thus, the dominant contribution to the cost of the calculating the EP at a single point scales linearly with the number of atoms in the nanocluster.

To summarize, we suggest a systematic way of constructing accurate electrostatic embedding potential for bulk, surfaces, and nanostructures of crystalline materials. To regularize the summation of the EP series, the original lattice cell is modified so as to eliminate its electric multipole moments up to any given \mathcal{M} and, thus, to make the potential produced by such a cell short range. We applied this method to several crystals, including complex minerals containing 50–100 atoms per cell, and demonstrated rapid convergence of the EP inside finite nanoscale clusters. The method is fully analytical, and the convergence can be controlled by a few well-defined numerical parameters.

Acknowledgment. The authors are grateful to A. L. Shluger for stimulating discussions and comments on the manuscript. P.V.S. is supported by the Royal Society. I.V.A.'s stay at University College London was supported by the Thomas Young Centre—the London Centre for Theory and Simulation of Materials—and by the EPSRC Grant no. GR/S80080/01. The calculations have been performed on the computer cluster funded via the Elements Science and Technology Project, MEXT, and Grant-in-Aid for Young Scientists 20810004 at the WPI-Advanced Institute for Materials Research, Tohoku University, Japan.

References

- Stefanovich, E. V.; Shidlovskaya, E. K.; Shluger, A. L.; Zakharov, M. A. *Phys. Stat. Sol. B* **1990**, *160*, 529.
- Abarenkov, I. V.; Bulatov, V. L.; Godby, R.; Heine, V.; Payne, M. C.; Souchko, P. V.; Titov, A. V.; Tupitsyn, I. I. *Phys. Rev. B: Condens. Matter Mater. Phys.* **1997**, *56*, 1743.
- Govind, N.; Wang, Y. A.; Carter, E. A. *J. Chem. Phys.* **1999**, *110*, 7677.
- Donnerberg, H.; Birkholz, A. *J. Phys.: Condens. Matter* **2000**, *12*, 8239.
- Sushko, P. V.; Shluger, A. L.; Catlow, C. R. A. *Surf. Sci.* **2000**, *450*, 153.
- Sherwood, P.; de Vries, A. H.; Guest, M. F.; Schreckenbach, G.; Catlow, C. R. A.; French, S. A.; Sokol, A. A.; Bromley, S. T.; Thiel, W.; Turner, A. J.; Billeter, S.; Terstegen, F.; Thiel, S.; Kendrick, J.; Rogers, S. C.; Casci, J.; Watson, M.; King, F.; Karlsen, E.; Sjovoll, M.; Fahmi, A.; Schfer, A.; Lennartz, C. *J. Mol. Struct.* **2003**, *632*, 1.
- Nasluzov, V. A.; Ivanova, E. A.; Shor, A. M.; Vayssilov, G. N.; Birkenheuer, U.; Rösch, N. *J. Phys. Chem. B* **2003**, *107*, 2228.
- Herschend, B.; Baudin, M.; Hermansson, K. *J. Chem. Phys.* **2004**, *120*, 4939.

- (9) Seijo, L.; Barandiarán, Z. *J. Chem. Phys.* **2004**, *121*, 6698.
- (10) Laino, T.; Mohamed, F.; Laio, A.; Parrinello, M. *J. Chem. Theory Comput.* **2006**, *2*, 1370.
- (11) Danyliv, O.; Kantorovich, L.; Cora, F. *Phys. Rev. B: Condens. Matter Mater. Phys.* **2007**, *76*, 045107.
- (12) Kästner, J.; Thiel, S.; Senn, H. M.; Sherwood, P.; Thiel, W. *J. Chem. Theory Comput.* **2007**, *3*, 1064.
- (13) Higashi, M.; Truhlar, D. G. *J. Chem. Theor. Comput.* **2008**, *4*, 790.
- (14) Burow, A. M.; Sierka, M.; Döbler, J.; Sauer, J. *J. Chem. Phys.* **2009**, *130*, 174710.
- (15) Kamerlin, S. C. L.; Haranczyk, M.; Warshel, A. *J. Phys. Chem. B* **2009**, *113*, 1253.
- (16) Lin, H.; Truhlar, D. G. *Theor. Chem. Acc.* **2007**, *117*, 185.
- (17) Komin, S.; Gossens, C.; Tavernelli, I.; Rothlisberger, U.; Sebastiani, D. *J. Phys. Chem. B* **2007**, *111*, 5225.
- (18) McKenna, K. P.; Sushko, P. V.; Shluger, A. L. *J. Am. Chem. Soc.* **2007**, *129*, 8600.
- (19) Kimmel, A. V.; Sushko, P. V.; Shluger, A. L.; Kuklja, M. M. *J. Phys. Chem. A* **2008**, *112*, 4496.
- (20) Torras, J.; Bromley, S.; Bertran, O.; Illas, F. *Chem. Phys. Lett.* **2008**, *457*, 154.
- (21) Shluger, A. L.; Sushko, P. V.; Kantorovich, L. N. *Phys. Rev. B: Condens. Matter Mater. Phys.* **1999**, *59*, 2417.
- (22) Govind, N.; Sushko, P. V.; Hess, W. P.; Valiev, M.; Kowalski, K. *Chem. Phys. Lett.* **2009**, *470*, 353.
- (23) Pacchioni, G.; Valentini, C. D.; Dominguez-Ariza, D.; Illas, F.; Bredow, T.; Kluner, T.; Staemmler, V. *J. Phys.: Condens. Matter* **2004**, *16*, S2497.
- (24) Sousa, C.; de Graaf, C.; Lopez, N.; Harrison, N. M.; Illas, F. *J. Phys.: Condens. Matter* **2004**, *16*, S2557.
- (25) Giordano, L.; Sushko, P. V.; Pacchioni, G.; Shluger, A. L. *Phys. Rev. Lett.* **2007**, *99*, 136801.
- (26) Müller, M.; Stankic, S.; Diwald, O.; Knözinger, E.; Sushko, P. V.; Trevisanutto, P. E.; Shluger, A. L. *J. Am. Chem. Soc.* **2007**, *129*, 12491.
- (27) Bo, C.; Maseras, F. *Dalton Trans.* **2008**, *22*, 2911.
- (28) Kantorovich, L. N.; Shluger, A. L.; Sushko, P. V.; Günster, J.; Stracke, P.; Goodman, D. W.; Kemper, V. *Faraday Discuss.* **1999**, *114*, 173.
- (29) Sushko, P. V.; Gavartin, J. L.; Shluger, A. L. *J. Phys. Chem. B* **2002**, *106*, 2269.
- (30) Ricci, D.; Valentini, C. D.; Pacchioni, G.; Sushko, P. V.; Shluger, A. L.; Giamello, E. *J. Am. Chem. Soc.* **2003**, *125*, 738.
- (31) Sterrer, M.; Diwald, O.; Knözinger, E.; Sushko, P. V.; Shluger, A. L. *J. Phys. Chem. B* **2002**, *106*, 12478.
- (32) Sterrer, M.; Berger, T.; Diwald, O.; Knözinger, E.; Sushko, P. V.; Shluger, A. L. *J. Chem. Phys.* **2005**, *123*, 064714.
- (33) Beck, K. M.; Henyk, M.; Wang, C.; Trevisanutto, P. E.; Sushko, P. V.; Hess, W. P.; Shluger, A. L. *Phys. Rev. B: Condens. Matter Mater. Phys.* **2006**, *74*, 045404.
- (34) Beck, K. M.; Joly, A. G.; Diwald, O.; Stankic, S.; Trevisanutto, P. E.; Sushko, P. V.; Shluger, A. L.; Hess, W. P. *Surf. Sci.* **2008**, *602*, 1968.
- (35) Contact authors for a stand alone Fortran 77 code generating charges $e(\mathbf{n})$ for an arbitrary lattice.
- (36) Abarenkov, I. V. *Phys. Rev. B: Condens. Matter Mater. Phys.* **2007**, *76*, 165127.
- (37) Evjen, H. M. *Phys. Rev.* **1932**, *39*, 675.
- (38) Wolf, D.; Kebbinski, P.; Phillipot, S. R.; Eggebrecht, J. *J. Chem. Phys.* **1999**, *110*, 8254.
- (39) Sherwood, P.; de Vries, A. H.; Collins, S. J.; Greatbanks, S. P.; Burton, N. A.; Vincent, M. A.; Hillier, I. H. *Faraday Discuss.* **1997**, *106*, 79.
- (40) Stefanovich, E. V.; Truong, T. N. *J. Phys. Chem. B* **1998**, *102*, 3018.
- (41) French, S. A.; Sokol, A. A.; Bromley, S. T.; Catlow, C. R. A.; Rogers, S. C.; King, F.; Sherwood, P. *Angew. Chem., Int. Ed. Engl.* **2001**, *40*, 4437.
- (42) Teunissen, E. H.; Jansen, A. P. J.; van Santen, R. A.; Orlando, F. L.; Dovesi, R. *J. Chem. Phys.* **1994**, *101*, 5865.
- (43) Nam, K.; Gao, J.; York, D. M. *J. Chem. Theory Comput.* **2005**, *1*, 2.
- (44) Ewald, P. P. *Ann. Phys. (Leipzig)* **1921**, *64*, 253.
- (45) Porto, M. *J. Phys. A: Math. Gen.* **2000**, *33*, 6211.
- (46) Madelung, E. *Phys. Z.* **1918**, *19*, 524.
- (47) Kudin, K. N.; Scuseria, G. E. *Chem. Phys. Lett.* **1998**, *283*, 61.
- (48) Ramo, D. M.; Sushko, P. V.; Gavartin, J. L.; Shluger, A. L. *Phys. Rev. B: Condens. Matter Mater. Phys.* **2008**, *78*, 235432.
- (49) When the original unit cell is shifted to place the main vertex of a tetrahedron $T_{\mathcal{M}}^a$ to the origin, some components of its multipole moments can accidentally become equal to zero. In this case, the number of charges $e(\mathbf{n})$ can also reduce. In our calculations, this was the case for the rutile lattice and $v = -1.0$ (see Figure 6b).
- (50) Tupizin, I. I.; Abarenkov, I. V. *Phys. Stat. Sol. B* **1977**, *82*, 99.
- (51) Smith, E. R. *Proc. R. Soc. London, Ser. A* **1981**, *375*, 475.
- (52) Kantorovich, L. N.; Tupitsyn, I. I. *J. Phys.: Condens. Matter* **1999**, *11*, 6159.

CT900480P